Evanescent excitation and collection of spontaneous Raman spectra using silicon nitride nanophotonic waveguides

Ashim Dhakal[1,2*], Ananth Z. Subramanian[1,2], Pieter Wuytens[1,2,3], Frédéric Peyskens[1,2], Nicolas Le Thomas[1,2] and Roel Baets[1,2]

[1]*Photonics Research Group, INTEC Department, Ghent University–imec, Belgium*
[2]*Center for Nano- and Biophotonics, Ghent University, Belgium*
[3]*Department of Molecular Biotechnology, Ghent University–imec, Belgium*
**Corresponding author: ashim.dhakal@intec.ugent.be*

Received April 28, 2014

We experimentally demonstrate the use of high contrast, CMOS-compatible integrated photonic waveguides for Raman spectroscopy. We also derive the dependence of collected Raman power with the waveguide parameters and experimentally verify the derived relations. Isopropyl alcohol (IPA) is evanescently excited and detected using single-mode silicon-nitride strip waveguides. We analyze the measured signal strength of pure IPA corresponding to 819 cm^{-1} Raman peak due to in-phase C-C-O stretch vibration for several waveguide lengths, and deduce a pump power to Raman signal conversion efficiency on the waveguide to be at least 10^{-11} per cm.

OCIS Codes: (130.0130) Integrated optics; (300.6450) Raman spectroscopy; (230.7380) Waveguides, channeled; (130.6010) Integrated Optics, Sensors; (290.5860) Raman scattering; (280.0280) Optical sensing and sensors
http://dx.doi.org/10.1364/OL.99.09999

Raman spectroscopy is a key technique for the detection and analysis of trace substances in applications ranging from physics and chemistry to biology and environmental sciences. However, Raman spectroscopic techniques often require bulky and/or expensive instrumentation to overcome the inherently weak nature of the Raman scattering process [1]. Typical spontaneous Raman spectroscopic systems use a microscopy system or a free space beam. These systems suffer from a poor conversion efficiency (defined as the signal to pump power ratio), mainly due to small interaction volume and poor efficiency of signal collection. To overcome the difficulties with these systems, waveguide-based systems have been demonstrated in the form of hollow fibers for Raman spectroscopy of gases [2] or liquid core waveguides for liquids [3]. In this letter, we demonstrate the use of integrated singlemode silicon nitride (Si_3N_4) waveguides [4] for excitation, collection, and enhancement of the Raman signal using the evanescent field of the guided mode. We envision that using mature photonic integration technologies [5-6] a complete Raman spectroscopic system can be integrated on a CMOS-compatible chip. In addition to the reduction of cost and size of the instrumentation, the reduced mode area due to the use of high contrast nanophotonic waveguides also boosts the Raman signal. Based on our theoretical calculations [7-8], the use of a singlemode high contrast waveguide enhances the Raman signal by at least a factor of 500 per cm of waveguide length compared to the confocal microscopy systems. The use of cavities and nanoplasmonic structures defined on the waveguides [9] can further enhance the signal significantly. In this letter, we outline the theory of using the evanescent field of single mode photonic waveguides for Raman sensing and report the first experimental demonstration thereof.

An emitting molecule can be modelled as a dipole oscillating at a frequency c/λ_0. We consider that the molecule is located at the position $\boldsymbol{r}_0$ in the neighborhood of a photonic waveguide. Using Fermi's golden rule in a semi classical approach, the power coupled to a waveguide mode from the dipole can be calculated to be [10]:

$$\frac{P_{wg}(\vec{r}_0)}{P_0} = \frac{3}{4\pi}\frac{n_g}{n}\left(\frac{\lambda_0}{n}\right)^2 \frac{\varepsilon(\vec{r}_0)\left|\hat{d}_0 \bullet \vec{E}(\vec{r}_0)\right|^2}{\iint \varepsilon_0 \varepsilon(\vec{r})\left|\vec{E}(\vec{r})\right|^2 d\vec{r}} \qquad (1)$$

where n_g is the group index of the mode, n the refractive index at the location of the molecule, $\varepsilon(\boldsymbol{r})$ is the relative permittivity, $\hat{d}_0$ is the unit vector along the dipole, and $\mathbf{E}$ is the electric field strength of the mode. $P_0 = \omega^4|\boldsymbol{d_0}|^2 /(12\pi\varepsilon_0 c^3)$ is the power radiated by the dipole with dipole strength $\boldsymbol{d_0}$ in free space. Now we assume that the dipole has a scalar polarizability α, and is excited by a pump travelling in the same waveguide with power P_{pump} and a frequency sufficiently near to c/λ_0. Then, using the normalization of the guided mode and its power [11], $\left|d_0\right|^2 = \alpha^2\left|E(\vec{r}_0)\right|^2 \frac{n_g P_{pump}}{\iint c\varepsilon_0 \varepsilon(\vec{r})\left|E(\vec{r})\right|^2 d\vec{r}}$; hence,

$$\frac{P_{wg}(r_0)}{P_{pump}} = \frac{\pi^2}{n}\left(\frac{\left|E(\vec{r}_0)\right|^2}{\iint \varepsilon_0 \varepsilon(\vec{r})\left|E(\vec{r})\right|^2 d\vec{r}}\frac{\alpha n_g}{\lambda_0}\right)^2 \equiv \eta(r_0)\sigma \qquad (2)$$

where we have used the quadratic relationship between the polarizability and the scattering cross section σ [1]. Note that Eq. (2) describes the overall efficiency, as a combined efficiency of excitation and collection, whereby waveguide enhancement effects [7-8] are taken into account. To arrive at Eq. (2), we have neglected the Stokes shift between the pump and the Raman signal. This has no significant impact on the analysis and conclusions that follow.

We now assume that the scattering molecules are suspended uniformly in the upper cladding of the waveguides with a density ρ. For emitters forming a thin sheet of thickness dz orthogonal to the waveguide and covering the entire cladding area (see Fig. 1), the efficiency is given by the sum of the individual contributions:

$$\frac{dP_{wg}}{P_{pump}} = dz\rho\sigma \iint_{clad} \eta(\vec{r})d\vec{r} = dz\rho\sigma\eta_0 \tag{3}$$

where $\eta_0=\iint\eta(\boldsymbol{r})d\boldsymbol{r}$ is the *specific conversion efficiency* of the waveguide. This unitless parameter depends only on the electromagnetic conditions and the geometry of the waveguide, which can be solved using mode solvers. Using the COMSOL finite element mode solver, the value of η_0 for the Si_3N_4 strip waveguides used for the experiments [4] in this letter was estimated to be $6.4\text{x}10^{-2}$ for a 785 nm pump for the TE fundamental mode of the waveguide. This value leads to a conversion efficiency ($\rho\sigma\eta_0$) of $4\text{x}10^{-10}$/cm [8] for pure IPA. Here, we have taken a cross-section of $7.9\text{x}10^{-31}$ cm^2/sr^{-1} for the 819 cm^{-1} line due to C-C-O stretch vibration which is calculated using the value provided in [12] and using the $1/\lambda_0^4$ dependence of the cross-section[1].

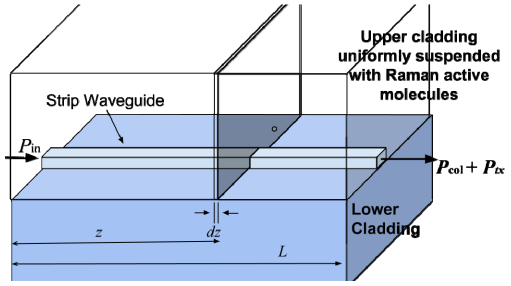

Fig. 1: Schematic of our analysis applied to the strip waveguide geometry. The particles are assumed to be embedded with a uniform density on the upper cladding. Symbols are explained in the text.

Although we have assumed that the entire upper cladding is covered by the Raman active molecules, a 350 nm thick layer of analyte is sufficient to produce an equivalent result, as the interaction takes place with exponentially decaying evanescent tail of the mode in the cladding with $1/e$ length less than 250 nm.

We now consider a practical situation, as depicted in Fig. 1. A pump laser with power P_{in} is incident on the input facet of the waveguides, of which a fraction gets coupled to the waveguide mode with coupling efficiency γ_{in} and propagates along the waveguide. During the propagation, molecules in the cladding are excited, and the scattered spontaneous Raman signal is collected via evanescent coupling to the same waveguide, as described by Eq. (3) in both forward and backward propagating directions. In the forward propagating configuration, only half of the collected power is measured at the output facet with an output coupling efficiency γ_{out}. Accounting for coupling losses and attenuation of the pump and collected signal in the waveguide, the ratio of signal power collected (P_{col}) at the end of the waveguide to the input power (P_{in}) is given by:

$$\begin{aligned}\frac{P_{col}(L)}{P_{in}} \equiv \xi(L) &= \rho\sigma\eta_0\gamma_{in}\gamma_{out}\int_0^L e^{-\alpha_p z}e^{-\alpha_s(L-z)}dz \\ &= \rho\sigma\eta_0\gamma_{in}\gamma_{out}e^{-\alpha_p L}\left[\frac{e^{\Delta\alpha L}-1}{\Delta\alpha}\right]\end{aligned} \tag{4}$$

where α_p, and α_s are the waveguide losses at the pump wavelength and at the Stokes wavelength respectively and $\Delta\alpha = \alpha_p$-α_s is their difference. The term in brackets evolves to L when $\Delta\alpha \rightarrow 0$.

If we assume that the coupling efficiencies from the waveguide end to the detector are equal for the pump and the Stokes signal, the Raman power collected at the end of the waveguide can be expressed in terms of the transmitted pump power (P_{tx}) at the detector, which can be directly measured. Thus, for many practical cases, it is convenient to define a quantity $\zeta(L)$ that is independent of coupling and waveguide losses:

$$\zeta(L) \equiv \frac{P_{col}(L)}{P_{tx}(L)} = \rho\sigma\eta_0\left[\frac{e^{\Delta\alpha L}-1}{\Delta\alpha}\right] \tag{5}$$

Along with Eq (2), Eq. (4) and (5) are the main theoretical results of this letter and express how the collected signal power depends on the input or transmitted pump power. In many situations, the quantity $\xi(L)$ is of practical interest, as the direct measure of the collected power for a given input power. However, it depends on coupling efficiencies and waveguide loss, which vary in the experiments. The quantity $\zeta(L)$ is independent of the coupling and the waveguide loss and can be used for purposes of direct analysis of signal strength with respect to concentration, cross-section, waveguide geometry and length. We will use both of these quantities to experimentally investigate the dependence of the Raman signal with the waveguide length.

The experimental setup is illustrated in Fig 2. A tunable Ti-Sapphire CW laser was used as the pump source. For the experiments, a wavelength of 785 nm is coupled to the waveguide by end-fire coupling using an aspheric lens of effective focal length 8 mm (NA=0.5). The Raman signal (Stokes) co-propagating with the pump that is collected by the waveguide is then collimated via an achromat objective (50x, NA=0.9) towards an edge filter, with the

edge wavelength at 795 nm to block pump light going into the spectrometer. The Raman signal is then focused to a single-mode optical fibre (cutoff =770 nm) using a parabolic mirror of 15 mm effective focal length (NA=0.2) and measured using a commercial spectrometer (AvaSpec-ULS2048XL).

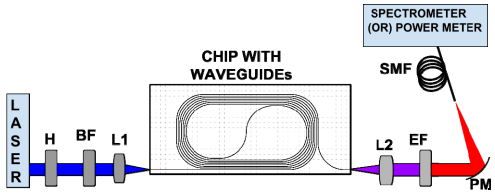

Fig 2: The schematic of experimental setup. *H:* half-waveplate, *BF:* Band-pass filter, *L1:* Aspheric lens. *L2:* Objective, *EF:* Long pass edge filter, *PM:* parabolic mirror, *SMF:* single-mode fibre

We use a Si_3N_4 waveguide (cross section: 700 nm x 220 nm) [4] on top of a 2.4 µm silica cladding on a silicon substrate as our sensing platform. Several waveguides of lengths 0.7 cm, 1.6 cm, 2.5 cm, 4.4 cm and 8.1 cm wound up to form spirals (typical physical widths of the spiral is 200 µm and the length of the spiral is about 625 µm per cm of waveguide length, bend radii of 25, 35, 50, 75 and 100 µm were used, bend losses for all of the spirals are negligible) are used as the sensing region for the experiment. The laser power is set to 90 mW, the polarization of the laser is set to couple into the TE mode of the waveguides. The laser is coupled to the waveguide with estimated total coupling loss from laser to detector (hence including both the in-coupling as well as the chip-fibre coupling) of 14±2 dB. Because of the edge filter, the pump transmission is measured and optimized at 800 nm wavelength which was verified to be practically the same as for the pump wavelength 785 nm without the filter.

A droplet of IPA is used as an analyte and is applied on top of the waveguides to cover the entire waveguide region. We ensure that IPA covers the entire waveguide by visually monitoring the chip with a camera on top. The spectra were recorded before and after application of IPA, as shown in Fig. 3. Before application of IPA we see a broad Raman emission in the range 2100-2400 cm^{-1} with a peak around 2330 cm^{-1} (960 nm). Based on the measurements with a confocal Raman microscope operating with 532 nm pump, this peak is identified as Raman emission from the Si_3N_4 material that forms the waveguide core. Another feature of the spectrum is the broad luminescence below 1200 cm^{-1} from the waveguide material. Immediately after application of IPA, the intense Raman peak at 819 cm^{-1} (839 nm) due to the in-phase C-C-O stretch vibration [13] is readily observed. The complete spectrum due to IPA is then extracted using the difference of the normalized spectrum before and after application of IPA. Since there is a difference in the modal properties of the waveguide before and after application of IPA, simply subtracting the spectra will not yield the desired spectrum of IPA. First, there is an increase in the transmitted pump and signal power after application of IPA. This is due to reduced sidewall scattering contribution to the waveguide losses because the cladding index has significantly changed (refractive index of IPA =1.377). Second, the confinement of the mode in the waveguide core and cladding changes, leading to a modified background contribution from the corresponding materials. To account for the change in the intensity due to decreased waveguide losses, we normalize the two spectra with the respective intensities corresponding to the peak due to Si_3N_4 at 2330 cm^{-1}. This also ensures that the invariant part of the background contributions from the waveguide core measured before application of IPA is removed when we subtract the normalized spectra before and after application of IPA. The residual background due to the changes in the cladding conditions is removed by fitting the remainder spectrum with truncated polynomials [14]. The resultant spectrum is then converted back to original units using the corresponding counts of the 2330 cm^{-1} peak used for normalization. The resultant spectrum, as we can see in Fig. 3 b), matches with the spectrum of IPA measured independently [15].

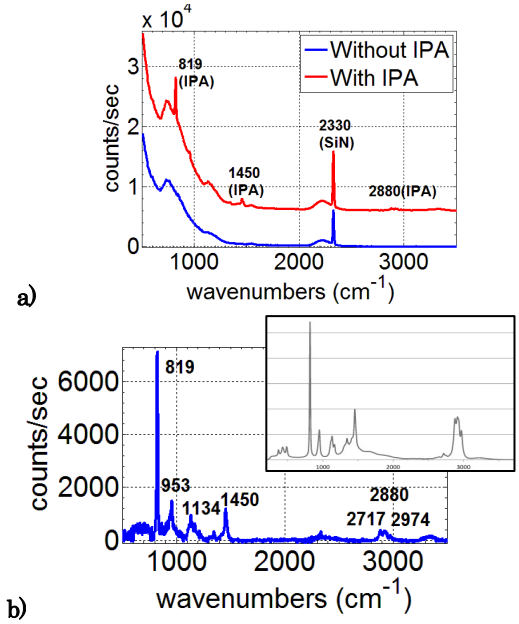

Fig 3: **a)** Raw spectrum measured from a 1.6 cm waveguide without IPA (blue) and with IPA (red). The spectra are shifted vertically for clarity with respective zeros at 3500 cm^{-1}. **b)** The spectrum of IPA extracted from the spectra in Fig 3(a). The spectrum measured independently using a commercial spectrometer is also shown in the inset (from [15]).

Fig. 4 a) shows the measured $\xi(L)$ for the 817 cm^{-1} peak due to the IPA for several waveguide lengths. Ten different sets of waveguide samples with different lengths were used for the measurements. The average and standard deviation of the measured $\xi(L)$ and the curve for Eq. (4) that fits the averages with the least squared error is also shown as a guide to the eye. The results follow the trend described by Eq. (4), in spite of considerable standard deviation due to differences in the quality of the

waveguide facets, the particles stuck on the waveguides during cleaving and imperfections in waveguide processing. The waveguide loss calculated from the transmission data using cutback method, 2.1±0.4 dB/cm is very close to the value 2.2 dB/cm obtained from the least square fit of Eq. (4). We see that the optimal waveguide length for $\xi(L)$ is given by $L=1/\alpha$, as can be inferred from Eq. (4)

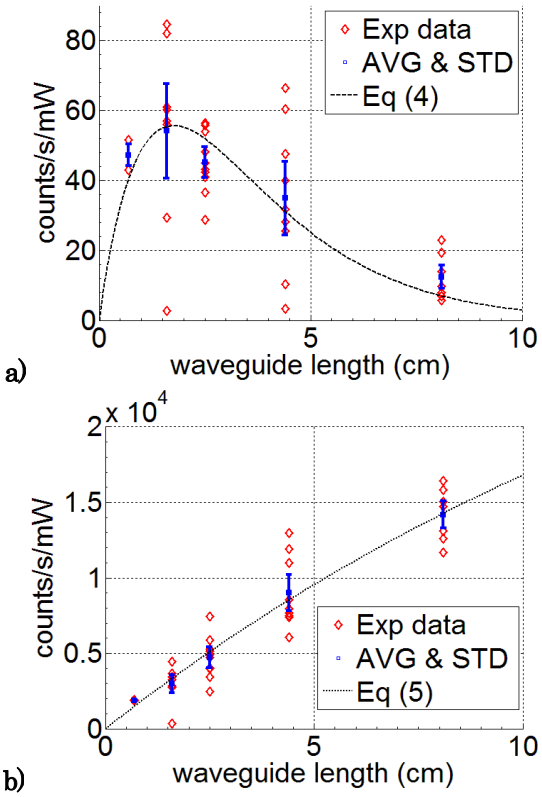

Fig 4: **a)** $\xi(L)$ and **b)** $\zeta(L)$ for 819 cm^{-1} peak due to IPA measured using photonic waveguides of several lengths. *Red diamond markers:* actual measured data, *Blue solid square with error bars*: mean and standard deviation, *Black dashed line*: theoretical fit, to respective equations as a guide for the eye.

In Fig. 4 (b) we show the measured $\zeta(L)$ for the IPA peak at 819 cm^{-1}. As expected from Eq (5), for $\Delta\alpha \approx 0$, we see a quasi-linear trend. Using the least squared error fit, the value of $\rho\sigma\eta_0$ for the IPA-waveguide system was extracted to be 2200 counts/s per mW of transmitted pump power per cm waveguide. $\Delta\alpha$ was extracted to be 0.2 dB/cm, which is equal to the measured value within the limits of experimental errors. As seen in Fig. 4, unlike the parameter $\xi(L)$, which depends on coupling and waveguide losses hence suffers from a large variance, $\zeta(L)$ has smaller variance and is suitable for directly assessing the specific efficiency of Raman scattering with the waveguide mode as defined by Eq. (5).

Using the measured sensitivity of the spectrometer in our configuration (in the order of 100 counts/ms/pW), the value of $\rho\sigma\eta_0$ can be calculated to be in the order of 10^{-11}/cm. Thus, the measured value of conversion efficiency $\rho\sigma\eta_0$ is about one order of magnitude lower than the value estimated in the theoretical section. This is a reasonable correspondence given the combination of uncertainties on the scattering cross-section and the measurement error.

To conclude, we have experimentally demonstrated Raman spectroscopy on a chip using single mode integrated optical waveguides, by exploiting enhanced light scattering due to the strong confinement in high index contrast waveguides as well as the long interaction length of the waveguide mode with the analyte in the cladding. Further, we have developed a theory for excitation and collection of spontaneous Raman signal using the photonic waveguides and identified the relevant parameters of interest η_0, $\xi(L)$ and $\zeta(L)$. For a given pump power within a typical single mode nanophotonic Si_3N_4 waveguide discussed in [4], we report a conversion efficiency in the order of 10^{-11}/cm for the 819 cm^{-1} Raman line of IPA.

The authors acknowledge the ERC advanced grant InSpectra for partial funding and imec, Leuven for processing of the waveguides

References.

1. D. A. Long, The Raman Effect: A Unified Treatment of the Theory of Raman Scattering by Molecules, J Wiley & Sons, Ltd, Chichester, UK (2002)
2. M. P. Buric, K. P. Chen, J. Falk, and S. D. Woodruff, Appl. Opt. **47**, 23 (2008)
3. J.S.W. Mak, S.Rutledge, R.M. Abu-Ghazalah, F. Eftekhari, J. Irizar, N.C.M. Tam, G. Zheng, A. S. Helmy, Prog. Quant. Elec. **37** (2013)
4. A. Z. Subramanian, P. Neutens, A. Dhakal, R. Jansen, T. Claes, X. Rottenberg, F. Peyskens, S. Selvaraja, P. Helin, B. Du Bois, K. Leyssens, S. Severi, P. Deshpande, R. Baets, P. Van Dorpe, IEEE Photonics J., **5**, 2202809 (2013)
5. D. Dai, J. Bauters, and J.E. Bowers, Light: Sci. Appl. **1**, 1 (2012)
6. M. Pollnau, N. Ismail, B.I. Akca, K. Wörhoff, R.M. de Ridder; Proc. SPIE 8266, Silicon Photonics VII (2012)
7. A. Dhakal, A.Z. Subramanian, N. Le Thomas, R. Baets, 16th European Conf. on Integrated Optics, Spain (2012)
8. A. Dhakal, F. Peyskens, A.Z. Subramanian, N. Le Thomas, R. Baets, Advanced Photonics Congress, PR, USA (2013)
9. F. Peyskens, A.Z. Subramanian, A. Dhakal, N. Le Thomas, R. Baets, CLEO, USA (2013)
10. Y.C. Jun, R.M. Briggs, H. A. Atwater, M.L. Brongersma, Opt. Express, **17**, 7479 (2009).
11. A.W. Snyder, J.D. Love, Optical Waveguide Theory, Chapman and Hall, New York, (1983).
12. M.J. Colles, J.E Griffiths. J. Chem. Phys., **7,** 56, (2003).
13. D Lin-Vien; N. B. Colthup; W. G. Fateley, J. G. Grasselli, The handbook of infrared and Raman characteristic frequencies of Organic Molecules, Academic Press, CA, (1991)
14. V. Mazet, C. Carteret, D. Brie, J. Idier, B. Humbert. Chemom. Intell. Lab. Syst. **76,** 2 (2005)
15. http://www.oceanoptics.com/images/spectra-isopropanol.jpg

References with title.

1. D. A. Long, 'The Raman Effect: A Unified Treatment of the Theory of Raman Scattering by Molecules', John Wiley & Sons, Ltd, Chichester, UK (2002)
2. M. P. Buric, K. P. Chen, J. Falk, and S. D. Woodruff, 'Enhanced spontaneous Raman scattering and gas composition analysis using a photonic crystal fiber', Appl. Opt. **47**, 23 (2008)
3. J.S.W. Mak, S.Rutledge, R.M. Abu-Ghazalah, F. Eftekhari, J. Irizar, N.C.M. Tam, G. Zheng, A. S. Helmy, 'Recent developments in optofluidic-assisted Raman spectroscopy', Prog. Quant. Elec. **37 1** (2013)
4. A. Z. Subramanian, P. Neutens, A. Dhakal, R. Jansen, T. Claes, X. Rottenberg, F. Peyskens, S. Selvaraja, P. Helin, B. Du Bois, K. Leyssens, S. Severi, P. Deshpande, R. Baets, P. Van Dorpe, 'Low-Loss Singlemode PECVD Silicon Nitride Photonic Wire Waveguides for 532–900 nm Wavelength Window Fabricated Within a CMOS Pilot Line'. IEEE Photonics J., **5**, 2202809 (2013)
5. D. Dai, J. Bauters, and J.E. Bowers, 'Passive technologies for future large-scale photonic integrated circuits on silicon: polarization handling, light non-reciprocity and loss reduction', Light: Sci. Appl. **1**, 1 (2012)
6. M. Pollnau, N. Ismail, B.I. Akca, K. Wörhoff, R.M. de Ridder, 'Biophotonic sensors on a silicon chip for Raman spectroscopy and optical coherence tomography', Proc. SPIE 8266, Silicon Photonics VII (2012)
7. A. Dhakal, A.Z. Subramanian, N. Le Thomas, R. Baets, 'The role of index contrast in the efficiency of absoprtion and emission of a luminescent particle near a slab waveguide', 16th European Conf. on Integrated Optics, Spain (2012)
8. A. Dhakal, F. Peyskens, A.Z. Subramanian, N. Le Thomas, R. Baets, 'Enhancement of light absorption, scattering and emission in high index contrast waveguides', Advanced Photonics Congress, PR, USA (2013)
9. F. Peyskens, A.Z. Subramanian, A. Dhakal, N. Le Thomas, R. Baets, 'Enhancement of Raman Scattering Efficiency by a Metallic Nano-antenna on Top of a High Index Contrast Waveguide', CLEO, USA (2013)
10. Y.C. Jun, R.M. Briggs, H. A. Atwater, M.L. Brongersma, 'Broadband enhancement of light emission in silicon slot waveguides', Opt. Express, **17**, 7479 (2009).
11. A.W. Snyder, J.D. Love, 'Optical Waveguide Theory', Chapman and Hall, New York, (1983).
12. M.J. Colles, J.E Griffiths, 'Relative and absolute Raman scattering cross sections in liquids', J. Chem. Phys., **7,** 56, (2003).
13. D Lin-Vien; N. B. Colthup; W. G. Fateley, J. G. Grasselli, 'The handbook of infrared and Raman characteristic frequencies of Organic Molecules' Academic Press, CA, pp 45-59 (1991)
14. V. Mazet, C. Carteret, D. Brie, J. Idier, B. Humbert, 'Background removal from spectra by designing and minimising a non-quadratic cost function', Chemom. Intell. Lab. Syst. **76,** 2 (2005)
15. http://www.oceanoptics.com/images/spectra-isopropanol.jpg